CrossMark

TECHNICAL PAPER

Self-sensing actuation for improved audio-induced vibration rejection in dual-stage hard disk drives

Bin Hu[1,2] · Jie Wan[2] · Chee Khiang Pang[1,3]

Abstract In this paper, a general circuit topology of enhanced indirect-driven self-sensing actuation (EIDSSA) is proposed to allow independent design of actuation and self-sensing in piezoelectric-actuated systems. Sensitivity analysis is performed in terms of suspension structural dynamics, geometric amplification and material property. The proposed EIDSSA circuit topology is realized and incorporated into a commercial dual-stage hard disk drive to improve the rejection capability of audio-induced vibrations. Experimental results show that the on-track total-runout has been reduced by 8.89% in pink noise audio-induced vibrations and 25.2% in single-tone 2.5 kHz audio-induced vibrations without additional loop tuning efforts.

1 Introduction

Piezoelectric materials find wide applications as sensors and actuators in mechatronic systems. Piezoelectric elements can be used as sensors attributing to the direct piezoelectric effect, where charges are generated upon deformation. They can also be employed as actuators owing to the converse piezoelectric effect, where deformation occurs with applied electric field (IEEE Standards on Piezoelectricity 1987). Thanks to

the fast response and high resolution, piezoelectric elements have gained huge popularity as actuators in nano-positioning systems, such as the Pb–Zr–Ti (PZT) actuators in hard disk drives (HDDs) and piezoelectric tube scanners in atomic force microscopy, to achieve high bandwidth and strong disturbance rejection (Kuiper et al. 2010; Li et al. 2011; Acosta et al. 2013; Hu et at. 2015). The controller design and driving mechanism have been extensively studied in the past decades (Nam et al. 2001; Vautier et al. 2005; Horowitz et al. 2007; Liu et al. 2013). Harnessing the reversibility of piezoelectric materials, self-sensing actuation technology allows piezoelectric elements to be used as actuators and sensors simultaneously. The concept is sprouted concurrently in the works of Dosch et al. (1992) and Anderson et al. (1992). Self-sensing actuators are naturally collocated and it has been shown that collocated control has a number of advantages relating to system stability. Self-sensing actuation also brings the benefits of weight and space reduction as well as cost saving.

Over the years, tremendous research efforts are devoted to study self-sensing actuation. Simmers et al. (2007) have investigated the thermal dependency of piezoelectric dielectric constant and proposed thermal protection. Asghari et al. (2015) have presented the effect of change in capacitance on self-sensing performance and improved the system stability with positive position feedback controller. Based on the circuit in Dosch et al. (1992), and Yamada et al. (2004) have designed active vibration controller by positive position feedback and direct velocity feedback in the PZT servo control loop. Pang et al. (2004) are the first to demonstrate the feasibility of self-sensing actuation in a dual-stage HDD servo system with critical resonances actively damped in a laboratory set-up. Other research works include various methods to improve the original bridge circuit, such as the work in Simmers et al. (2004) and Kuiper et al. (2010). Recently, indirect-driven

✉ Chee Khiang Pang
justinpang@nus.edu.sg

1 Department of Electrical and Computer Engineering, National University of Singapore, 4 Engineering Drive 3, Singapore 117583, Singapore

2 Singapore HDD R&D Centre, Western Digital Corporation, 89, Science Park Drive, Singapore Science Park 1, Singapore 118261, Singapore

3 Engineering Cluster, Singapore Institute of Technology, 20 Dover Drive, Singapore 138682, Singapore

self-sensing actuation (IDSSA) is developed to extend the sensing bandwidth and boost the SNR (Hong et al. 2012), but it suffers from gain loss and coupling effect causing the design of actuation and self-sensing to be highly dependent on each other.

Despite the aforementioned advantages, self-sensing actuation technology did not gain a lot of traction in the industry due to various concerns over prevailing solutions, such as SNR, plant gain loss and predominantly the coupling effect between self-sensing and actuation. The sensitivity of self-sensing signal to head displacement awaits to be established as special sensors. In this work, enhanced indirect-driven self-sensing actuation (EIDSSA) is proposed. We have successfully demonstrated the practicality of EIDSSA in practical dual-stage HDDs to improve the rejection capability of wide spectrum audio-induced vibrations. The sensitivity analysis is performed in piezoelectric-actuated systems to reveal design trade-offs in terms of physical dimensions and properties.

The remainder of this paper is organised as follows. Section 2 proposes the EIDSSA circuit topology to resolve coupling effects between actuation and self-sensing and discusses the sensitivity in piezoelectric-actuated systems. In Sect. 3, EIDSSA is evaluated experimentally and it is incorporated into a dual-stage HDD servo system to achieve stronger rejection of audio-induced vibration. Concluding remarks are given in Sect. 4.

2 Self-sensing actuation in piezoelectric-actuated systems

In this section, the circuit topology of enhanced indirect-driven self-sensing actuation (EIDSSA) is proposed and analyzed as compared to a conventional self-sensing circuit. Sensitivity analysis in PZT active suspensions is studied.

2.1 Proposed EIDSSA circuit topology

To realize the concept of self-sensing actuation, it is essential to decouple the effect due to the applied voltage from the output signal of the piezoelectric elements, leaving only the signal resulting from the strain. The decoupling operation is performed by a bridge circuit. A conventional bridge circuit for self-sensing actuation is shown in Fig. 1.

In Fig. 1, piezoelectric elements are modelled as self-sensing voltage V_p in series with equivalent capacitance C_p. Piezoelectric elements are direct-driven by the voltage V_{in}. The circuit can be analyzed by deriving the Laplace transforms of V_1 and V_2 as follows:

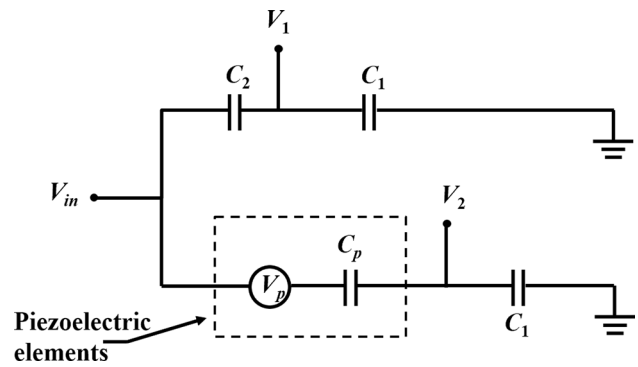$$V_1(s) = \frac{C_1}{C_1 + C_2} V_{in}(s), \tag{1}$$
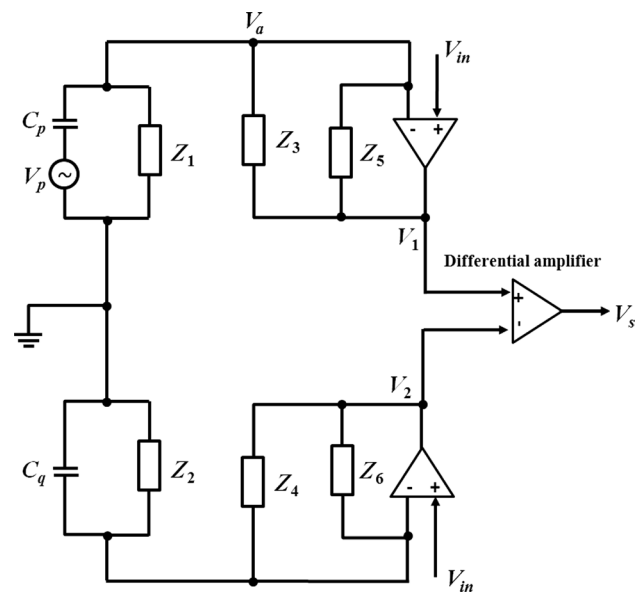

Fig. 1 Conventional bridge circuit

Fig. 2 Proposed EIDSSA circuit topology

$$V_2(s) = \frac{C_1}{C_1 + C_p}\left[V_{in}(s) - V_p(s)\right]. \tag{2}$$

The output $V_s(s)$ is obtained as

$$V_s(s) = V_2(s) - V_1(s)$$
$$= \left(\frac{C_1}{C_1 + C_2} - \frac{C_1}{C_1 + C_p}\right)V_{in}(s) + \frac{C_p}{C_p + C_2}V_p(s). \tag{3}$$

It is obvious that actuation efforts are not fully delivered to piezoelectric elements but by a factor of $C_p/(C_1 + C_p)$. The effects of actuation and self-sensing are coupled. Even if feed-through components are perfectly eliminated in $V_s(s)$ by choosing $C_2 = C_p$, $V_s(s)$ still cannot represent $V_p(s)$ well because $V_p(s)$ is attenuated by a factor of $C_1/(C_1 + C_p)$.

Since the magnitude of $V_p(s)$ is already very small, the attenuating effect results in further degraded SNR.

Based on the afore-going analysis, we propose the general circuit topology of EIDSSA as shown in Fig. 2.

In Fig. 2, Z_1–Z_6 denote impedances of particular nodes. Piezoelectric elements represented by V_p in series with C_p are indirect-driven by V_{in}. The impedances Z_1 and Z_2 are placed into the network aiming primarily to prevent the DC-drift phenomenon. V_a is the voltage delivered to piezoelectric elements. V_1 and V_2 are fed into a cascading system, which consists of a differential amplifier and its related electronics to produce output V_s. No electrical networks exist in the path from negative terminal of op-amps leading to the driving point.

The performance of the EIDSSA circuit can be parameterized according to the following equations:

$$\begin{cases} V_a = \gamma V_{in}, \\ V_s = (\alpha V_{in} + \beta V_p)\kappa, \end{cases} \tag{4}$$

where coefficients $\gamma = 100\%$, $\beta = \frac{Z_3 Z_5 C_p s}{Z_3 + Z_5}$, $\alpha = [\frac{Z_4 Z_6 (Z_2 C_q s + 1)}{Z_2 (Z_4 + Z_6)} - \frac{Z_3 Z_5 (Z_1 C_p s + 1)}{Z_1 (Z_3 + Z_5)}]$, and κ is determined by the design of differential amplifier. Coefficients α, β, γ, and κ describe decoupling, self-sensing, actuation, and amplification, respectively. If we choose $Z_1 = Z_2$, $Z_3 = Z_4$, $Z_5 = Z_6$, and $C_1 = C_p$, we have $\alpha = 0$.

Since $\gamma = 100\%$, the actuation in EIDSSA is gain-lossless. The design of self-sensing can be performed independently from actuation without coupling effects.

As the expression of β is made up of impedances Z_3, Z_5, and capacitance of C_p, impedances Z_1 and Z_2 do not contribute to the self-sensing performance. As Z_1–Z_6 are configurable, EIDSSA can be realized differently for various applications, such as displacement, velocity, and force sensing.

Design requirements can be specified by the set $S = \{\gamma, \beta, \kappa, \alpha\}$, where each element carries an explicit physical meaning. In general, a high-performance self-sensing circuit should possess the following properties:

1. γ should be 100% to ensure that control efforts are fully delivered to piezoelectric elements;
2. β should be close to 100% in the frequency range of interests so that V_s sufficiently represents V_p;
3. κ should be in a proper range to meet both SNR and sampling resolution requirements; and
4. α should be close to zero to ensure minimal feed-through components in V_s.

2.2 Sensitivity analysis in PZT active suspensions

In addition to self-sensing circuits, the design of self-sensing actuation requires considerations of mechanical properties of
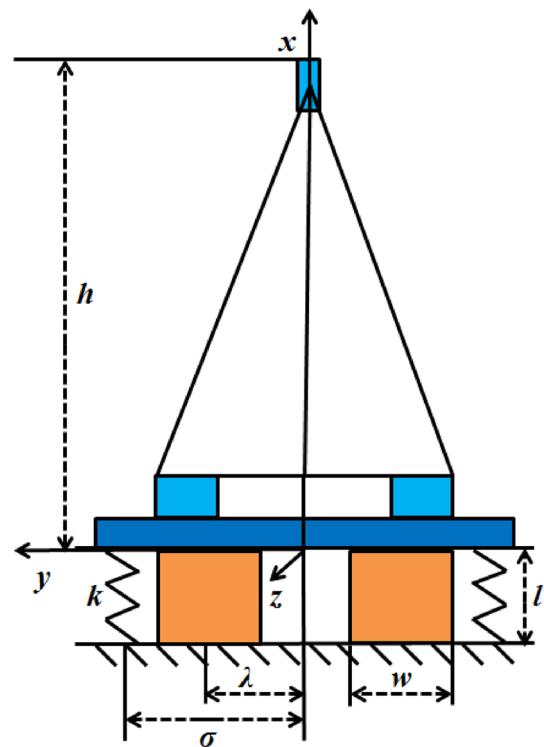

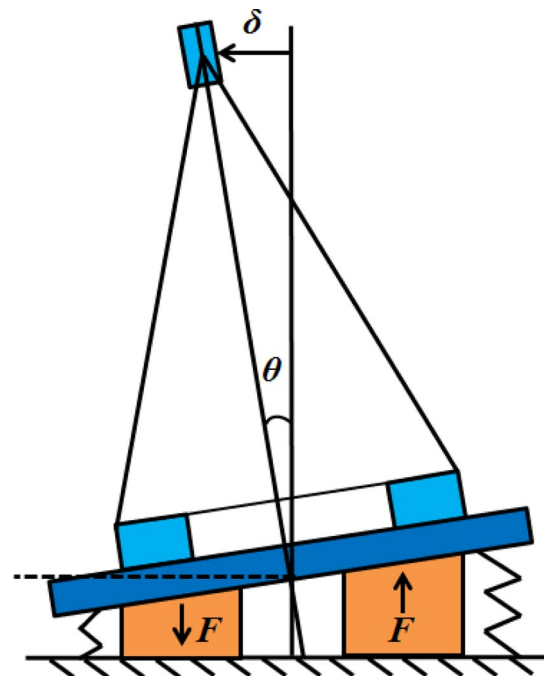**Fig. 3** Geometric relations in PZT active suspensions

Fig. 4 Off-track motion due to deformation of PZT elements

the piezoelectric-actuated system. Using the PZT active suspension in commercial dual-stage HDDs as an example, the sensitivity in piezoelectric-actuated systems is discussed.

The PZT active suspension can be approximated as a mass-spring damper system. The suspension stiffness is represented by two spring systems with stiffness k. The base plate is fixed and its movable mass including PZT elements and stiffener has an equivalent moment of inertia J. The geometric relations are defined in Fig. 3

In Fig. 3, w, l, and ρ are the width, length, and thickness of PZT elements, respectively. λ, σ, and h are distances from x-axis to the middle width of PZT element, from x-axis to the spring k, and from y-axis to head, respectively. In manufacturing, two PZT strips are polarized in opposite directions. When the electric field is applied, one strip shrinks in length and the other expands. Consequently, the suspension rotates by an angle θ for head displacement δ with reaction forces F from the springs, as shown in Fig. 4.

According to IEEE Standards on Piezoelectricity (1987), the electric displacement through the surface of PZT elements is given by

$$D_3 = d_{31}T_1 + \varepsilon_{33}^T E_3, \tag{5}$$

where D_3, d_{31}, T_1, ε_{33}^T, and E_3 are electric displacement, piezoelectric charge constant, stress, relative permittivity, and applied electric field, respectively. In piezoelectric relations, axes are identified by numerals rather than letters. The subscripts 1, 2, and 3 correspond to x-, y-, and z-axes herein.

Referring to Fig. 4, the dynamics of the suspension can be approximately described as

$$J\ddot{\theta} + 2k\sigma^2\theta = 2\lambda F, \tag{6}$$

where λ and σ are the distances from x-axis to the middle width of PZT element and to the spring, respectively.

The mechanical stress can be obtained from $T_1 = F/w\rho$, and we know $E_3 = V_{in}/\rho$. It follows that

$$D_3 = \frac{d_{31}}{w\rho}\left(\frac{J\ddot{\delta}}{2\lambda h} + \frac{k\sigma^2\delta}{\lambda h}\right) + \varepsilon_{33}^T\frac{V_{in}}{\rho}. \tag{7}$$

Electric charge across PZT elements can be obtained by calculating the surface integral of the scalar function D_3 defined on a bounded surface Φ as

$$Q = \iint_\Phi D_3\, d_\Phi = \frac{d_{31}l}{\rho}\left(\frac{J\cdot\ddot{\delta}}{2\lambda h} + \frac{k\sigma^2\delta}{\lambda h}\right) + \varepsilon_{33}^T\frac{wl}{\rho}V_{in}, \tag{8}$$

where Φ is the surface perpendicular to E_3 and the area of Φ equals to wl.

Since the two faces of PZT elements are coated with thin electrode layers, the capacitance can be determined from $C_p = \varepsilon_{33}^T wl/\rho$ (Moheimani et al. 2006).

V_p as the difference between the measured voltage and V_{in} can be derived as

$$V_p = \frac{d_{31}J}{2\lambda h\varepsilon_{33}^T w}\left(\ddot{\delta} + \frac{2k\sigma^2}{J}\delta\right). \tag{9}$$

In steady-state, we describe self-sensing sensitivity from V_p to δ as

$$S_s = \frac{V_p}{\delta} = \frac{d_{31}k\sigma^2}{\lambda h\varepsilon_{33}^T w} = \frac{\rho\lambda}{hl}\frac{d_{31}}{s_{11}^E\varepsilon_{33}^T}\left(\frac{\omega_p^2}{\omega_n^2 - \omega_p^2}\right), \tag{10}$$

where ω_p is the passive sway frequency obtained from (6) when $F = 0$ and ω_n is the suspension sway frequency in the free response when V_{in} is not present. ω_p and ω_n are identified by finite element analysis. The unit of S_s is mV/nm.

Similarly, the actuation sensitivity from δ to V_{in} has been derived by Liu et al. (2013) as

$$S_a = \frac{\delta}{V_{in}} = -\frac{h\lambda wld_{31}}{s_{11}^E k\sigma^2 l + w\rho\lambda^2} = -\frac{hl}{\rho\lambda}d_{31}\left(1 - \frac{\omega_p^2}{\omega_n^2}\right), \tag{11}$$

where the unit of S_a is nm/V.

Based on (10) and (11), we have the following design considerations of self-sensing actuation in PZT active suspensions:

- S_a increases while S_s decreases with greater geometric amplification factor as described by $hl/\rho\lambda$.
- Both S_a and S_s increase with larger d_{31}. S_s increases but S_a decreases with smaller ε_{33}^T.
- Larger S_a or stroke is achieved with smaller ratio of ω_p over ω_n. When $\omega_p \ll \omega_n$, S_a is obtained close to its maximum at $-d_{31}hl/\rho\lambda$. In this case, V_p is said to be insensible as $S_s \approx 0$.
- As d_{31} is negative, V_p should be in general out of phase with V_{in}. This out-of-phase relationship can be used as a quick rule for assessing if V_p is polluted by unwanted feed-through components from V_{in}.

Remark 1 It is worth nothing that the concepts of S_s and S_a apply to general piezoelectric-actuated systems. The expressions can be similarly derived with the results in (10) and (11) modified accordingly.

3 Experimental results and discussions

For demonstration purpose, a commercially available 3.5 inch dual-stage HDD with PZT active suspension is modified to integrate the proposed EIDSSA circuit as shown in Fig. 5. The same drive prior to any modifications is used to obtain baseline results without EIDSSA.
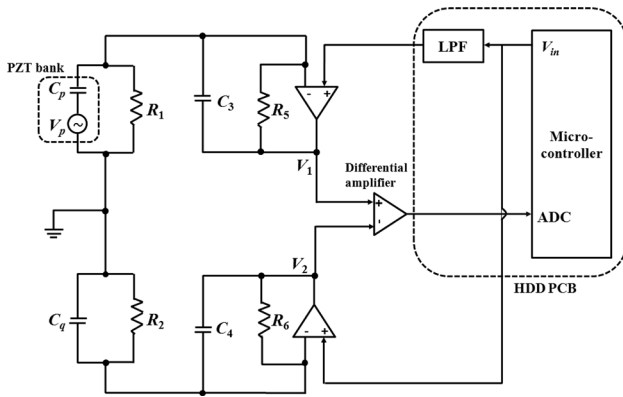
Fig. 5 Experimental set-up and system integration

Table 1 Values of circuit components

Component	Values
$R_1 = R_2$	1.0 MΩ
$C_3 = C_4$	1.25 nF
$R_5 = R_6$	560 kΩ
$C_p = C_q$	4.7 nF

Fig. 6 Time traces of V_s and V_{in}

Fig. 7 Bode diagrams of PZT active suspension

Fig. 8 High frequency mode detection by EIDSSA

Actuation sensitivity S_a can be obtained as the slope of PZT stroke measurement. According to our experiments, as V_{in} varies from 1 to 10 V, $S_a = 13.7$ nm/V. The time traces of V_s and V_{in} are plotted in Fig. 6.

With reference to Fig. 6, when V_{in} varies from -1.23 to 2.08 V, the head is displaced by $\delta = 13.7 \times [2.08 - (-1.23)] = 45.35$ nm. Correspondingly, V_s has changed from 1.91 to -3.04 V. With $\kappa = 30$ in our design, we obtain that $V_p = V_s/\kappa = (|-3.04 - 1.91|)/30 = 165$ mV. Hence, we have $S_s = V_p/\delta = 3.64$ mV/nm.

3.1 Evaluation of EIDSSA

The bode diagrams of PZT active suspension with EIDSSA and conventional IDSSA are presented in Fig. 7.

In Fig. 7, the bode diagram of PZT active suspension with EIDSSA shows no gain loss and almost no phase shift since $\gamma = 100\%$. However, gain reduction up to -6 dB below 10 kHz and significant phase shift in all frequencies are noticeable in the case of IDSSA with exact component values in Hong et al. (2012). When EIDSSA is directly applied, the total-runout (TRO) has been slightly improved by 0.8% according to our experiments. However, TRO is

With reference to Fig. 5, the impedances Z_1–Z_6 are realized into resistors R_1, R_2, R_5, R_6, and capacitors C_3, C_4, respectively. V_1 and V_2 are fed into the cascading differential amplifier. Output voltage V_s is routed to analog-to-digital-conversion (ADC) port of micro-controller for sampling. The low-pass-filter (LPF) represents a ferrite bead in the printed circuit board (PCB) to suppress unwanted noises in high frequencies due to electrical circuits. Bank-driving PZT actuators are connected in the upper arm of the proposed EIDSSA to achieve indirect-actuation. No plural of circuits is required for each head. The values of circuit components are tabulated in Table 1.
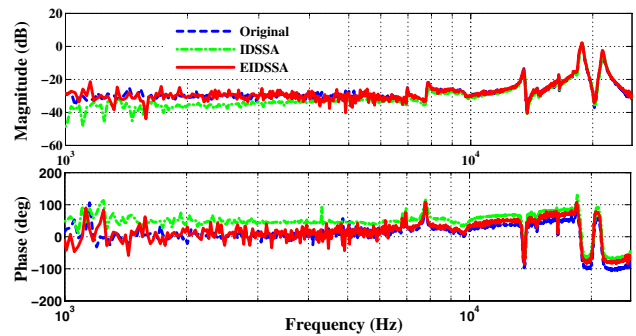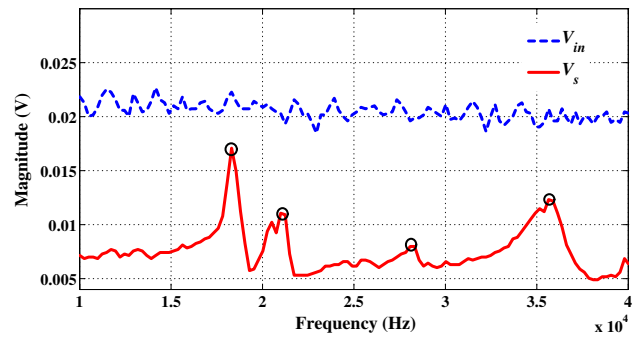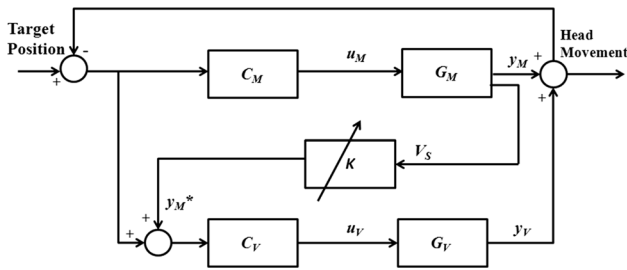
Fig. 9 Modified DMS servo control structure incorporating EIDSSA

Table 2 Stability margins and bandwidth in DMS servo

	Without EIDSSA	With EIDSSA
Gain margin	7.7 dB	7.8 dB
Phase margin	24°	36°
Bandwidth	2465 Hz	2765 Hz

doubled with IDSSA because of the gain loss and phase shift introduced by additional dynamics in the actuation path.

The output voltage V_s from EIDSSA contains rich signal contents in the frequency domain as shown in Fig. 8.

In Fig. 8, major off-track resonant modes at 18, 21 and 36 kHz are detected from V_s. The magnitude peaks correspond to resonant modes arising from the PZT active suspension. These modes are not excited by the input signal V_{in} but activated by various in-drive disturbances, such as the airflow resulting from disk rotation.

3.2 Control performance of dual-stage HDD servo incorporating EIDSSA

The block diagram of a modified decoupled master slave (DMS) servo incorporating EIDSSA mechanism is shown in Fig. 9.

In Fig. 9, denote voice coil motor (VCM) actuator as G_V, VCM controller as C_V, PZT actuator with the proposed EIDSSA as G_M, and PZT controller as C_M. u_M and u_V are PZT control and VCM control, respectively. y_M and y_V are the head displacement due to deformation of PZT elements and VCM motion, respectively. V_s from EIDSSA is transferred to y_M^* via a gain K which is obtained iteratively in firmware. As y_M^* actively decouples servo loops, standard controller design and loop shaping based on decoupled sensitivity can be carried out (Guo et al. 2003). Note that, in our work, high resolution PES is decoded from servo channel and the servo loops are closed in firmware.
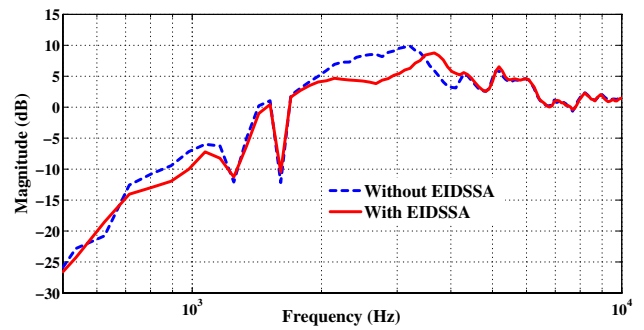
Fig. 10 Sensitivity transfer function of DMS servos
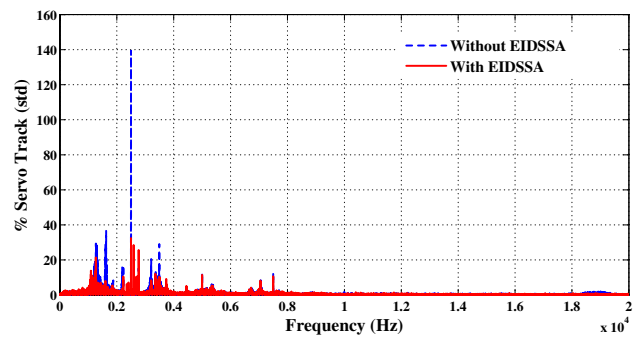
Fig. 11 NRRO when playing 2.5 kHz sinusoidal by vibration speaker

3.2.1 Bandwidth and stability

The bandwidth and stability margins of the new DMS servo incorporating EIDSSA are presented in Table 2.

From Table 2, the phase margin of the new system has gained from 24° to 36° with slightly improved gain margin. At the same time, servo bandwidth is extended by 300–2765 Hz in the modified DMS servo with EIDSSA. The higher bandwidth translates to stronger disturbance rejection capability during track-following operation. According to our experiments, the TRO, repeatable-runout (RRO), and non-repeatable-runout (NRRO) have been improved by 3.84, 4.07, and 2.97%, respectively.

3.2.2 Disturbance rejection capability

The disturbance rejection capability is analyzed by the sensitivity transfer function $1/(1 + C_M G_M)(1 + C_V G_V)$. The frequency response is presented in Fig. 10.

It is well known that linear systems are constrained by the famous waterbed effect. It is impossible to achieve an arbitrary sensitivity reduction at all points on the imaginary axis. From Fig. 10, the 0 dB crossover frequency is
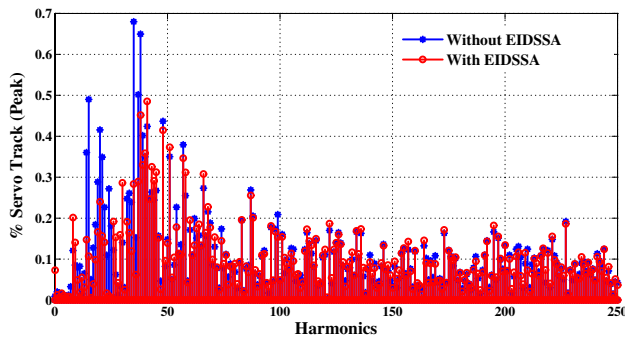
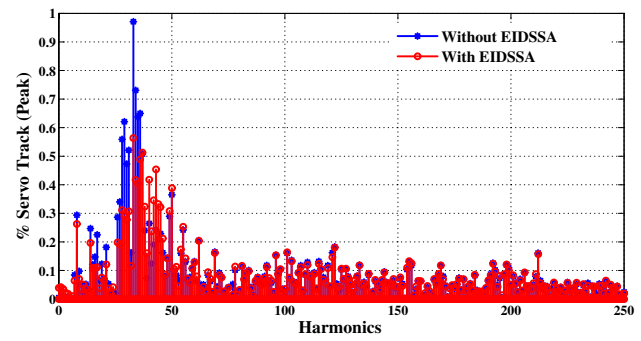**Fig. 12** RRO when playing 2.5 kHz sinusoidal by vibration speaker

Fig. 14 RRO when playing pink noise by vibration speaker labelfig
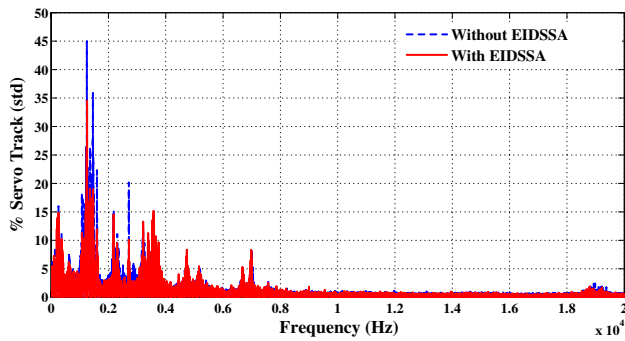

Fig. 13 NRRO when playing pink noise by vibration speaker

around 1.8 kHz, beyond which the sensitivity hump can be observed in the new system. It can be seen that the gain of sensitivity transfer function has been reduced by up to 5 dB from 2 to 3.5 kHz, while it increases from 3.5 to 4 kHz. There are also slight increases at higher frequencies which appear not obvious on the log-scale. Nevertheless, the peak value of the gain of sensitivity transfer function is still lower in the new system.

The results are highly desirable in real-world applications. The frequencies from 2 to 3 kHz fall into the typical range of audio-induced vibrations. In high-end HDD products, expensive vibrational sensors are often dedicatedly employed to improve the vibration rejection capability at these frequencies. With improved loop decoupling rendered by EIDSSA due to in-situ measurement of y_M^*, such desirable performance can be readily achieved with only a few additional cheap electronics.

Firstly, single tone sinusoidal signal at 2.5 kHz is applied to the base of HDD by a vibration speaker. The frequency of 2.5 kHz is chosen because it represents a typical frequency of audio-induced vibrations. The NRRO and RRO performances are presented in Figs. 11 and 12, respectively.

From Figs. 11 and 12, it can be seen that 2.5 kHz disturbance is suppressed significantly because of the lowered gain in sensitivity transfer function. Corresponding NRRO

and RRO have been improved by 29.9 and 13.2%, respectively. The TRO has been reduced by 25.2% as compared to the baseline DMS servo without EIDSSA.

Then, pink noise containing all frequencies from 20 Hz to 20 kHz is then applied to the base of HDD by vibration speaker to evaluate the audio-induced vibration rejection capability in a wider spectrum of frequencies. The results of NRRO and RRO are presented in Figs. 13 and 14.

Based on Figs. 13 and 14, the NRRO, RRO and TRO have been reduced by 7.92, 9.35, and 8.89%, respectively. Note that same source of audio is used for testing and sound level is maintained in each experiment. Experimental results have confirmed that the modified DMS servo with the proposed EIDSSA has achieved improved rejection of audio-induced vibrations.

4 Conclusion

In this paper, a general circuit topology of EIDSSA is proposed to achieve independent design of actuation and self-sensing. The sensitivity analysis in PZT active suspension is performed in terms of the physical dimensions and properties. EIDSSA is realized and incorporated into dual-stage HDD servos for stronger rejection capability of audio-induced vibrations. Experimental results show that total-runout (TRO) is reduced by 8.89% under pink noise and by 25.2% under single tone 2.5 kHz audio-induced vibrations without additional loop tuning efforts.

References

Acosta JC, Polesel-Maris J, Thoyer F, Xie H, Haliyo S, Regnier S (2013) Gentle and fast atomic force microscopy with a piezoelectric scanning probe for nanorobotics applications. Nanotechnology 24(6):1–11

Anderson EH, Hagood NW, Goodliffe JM (1992) Self-sensing piezoelectric actuation: analysis and application to controlled structures. In: Proceedings of the AIAA/ASME/ASCE/AHS/ASC

33rd structure, structural dynamics, materials conference. Dallas, Texas

Asghari M, Rezaei SM, Rezaie AH, Zareinejad M, Ghafarirad H (2015) Self-sensing actuation using online capacitance measurement with application to active vibration control. J Intell Mater Syst Struct 26(2):186–200

Dosch JJ, Inman DJ, Garcia E (1992) A self-sensing piezoelectric actuator for collocated control. J Intell Mater Syst Struct 3(1):166–185

Guo G, Wu D, Chong TC (2003) Modified dual-stage controller for dealing with secondary-stage actuator saturation. IEEE Trans Magn 39(6):3587–3592

Hong F, Pang CK (2012) Robust vibration control at critical resonant modes using indirect-driven self-sensing actuation in mechatronic systems. ISA Trans 51(6):834–840

Horowitz R, Li Y, Oldham K, Kon S, Huang X (2007) Dual-stage servo systems and vibration compensation in computer hard disk drives. Control Eng Pract 15(3):291–305

Hu B, Pang CK, Wan J, Kim Y-H, Tan JK (2015) Earliest switch-on of dual-stage actuation in hard disk drives. Microsyst Technol 22(6):1267–1273

IEEE Standard on Piezoelectricity (1987) ANSI/IEEE Standard 176–1987

Kuiper S, Schitter G (2010) Active damping of a piezoelectric tube scanner using self-sensing piezo actuation. Mechatronics 20(6):656–665

Li H, Du C, Wang Y (2011) Optimal reset control for a dual-stage actuator system in HDDs. IEEE/ASME Trans Mechatron 16(3):480–488

Liu Y (2013) Analytical dynamic model for suspension with PZT actuators. Microsyst Technol 19(9):1269–1274

Liu Y, Wang X, Lu Y (2013) Circuit model for piezoelectric actuator with electrically conductive epoxy. Microsyst Technol 19(9):1559–1565

Moheimani SOR, Fleming AJ (2006) Piezoelectric transducers for vibration control and damping. Springer Verlag, London Limited

Nam H, Cho S, Yee Y, Lee H, Kim D, Bu J, Hong J (2001) Fabrication and characteristics of piezoelectric PZT cantilever for high speed atomic force microscopy. Integr Ferroelectr 35(1):185–197

Pang CK, Guo G, Chen BM, Lee TH (2004) Nanoposition sensing and control in HDD dual-stage servo systems. In: Proceedings of the 2004 IEEE International CCA, 551–556, Taipei, Taiwan, September 2–4

Simmers GE, Hodgkins JR, Mascarenas DD, Park G, Sohn H (2004) Improved piezoelectric self-sensing actuation. J Intell Mater Syst Struct 15(12):941–953

Simmers GE, Sodano HA, Park G, Inman DJ (2007) Thermal protection for a self-sensing piezoelectric control system. Smart Mater Struct 16(6):2492–2500

Vautier BJG, Moheimani SOR (2005) Charge driven piezoelectric actuators for structural vibration control: Issues and implementation. Smart Mater Struct 14(4):575–586

Yamada H, Sasaki M, Nam Y (2004) Control of a micro-actuator for hard disk drives using self-sensing. Paper presented at 8th IEEE International Workshop on Advanced Motion Control